Automatic Intelligent Recognition of Pavement Distresses with Limited Dataset Using Generative Adversarial Networks

Zhuo Liu[a], Shuo Pan[a,*], Zhiwei Gao[b], Ning Chen[a], Feng Li[c], Linbing Wang[d], Yue Hou[e*]

[a] *Beijing Key Laboratory of Traffic Engineering, Beijing University of Technology, Beijing, 100124, China*

[b] *James Watt School of Engineering, University of Glasgow, Glasgow, G12 8LT, UK*

[c] *School of Transportation Science and Engineering, Beihang University, Beijing, 102206, China*

[d] *School of Environmental, Civil, Mechanical and Agricultural Engineering, University of Georgia, Georgia, USA.*

[e] *Department of Civil Engineering, Faculty of Science and Engineering, Swansea University, UK.*

* *Corresponding author. E-mail address: panshuo@emails.bjut.edu.cn (Shuo Pan); danielhou@ieee.org (Yue Hou).*

ABSTRACT

Automatic monitoring of pavement structure health has always been a significant problem for transportation engineers. Although the generative adversarial network (GAN) has proven to be an effective tool for improving pavement distress recognition accuracy, it may lead to increased computational cost, which inconsistent with the requirements of engineering practice. This paper describes a lightweight GAN structure for automatic pavement distress identification with high computation efficiency and low computation cost. Squeeze and expand (SE), multiscale convolution (MC), and depthwise separable convolution (DSC) were selected as alternative lightweight methods, and two series of comparative experiments were conducted. The results showed that the GAN-based model with SE implemented on its fully connected layer, MC&DSC implemented on its transpose convolution layers in the generator, and MC implemented on its convolution layers in the discriminator could reduce the largest proportion of model parameters (94.8%) while achieving satisfactory classification accuracy (85.4%).

Keywords: Automatic intelligent recognition, pavement distresses, Lightweight GAN, Multiscale convolution, Depthwise separable convolution

1 Introduction

Pavement distress significantly influences road safety, service quality, and service life, making pavement distress recognition crucial for road maintenance. Considering the substantial financial cost of field monitoring, image-based pavement distress recognition methods have been widely used in practical work owing to their acceptable cost and high efficiency. In the early stage, the collected distress images are usually processed by a preliminary step, which is to reduce the noise and adjust the contrast by histogram equalization [1]. The distress can be identified using algorithms such as the threshold algorithm [2] and region algorithm [3]. The main disadvantage of the traditional method is that the procedure is complex. To further realize the automatic classification of pavement distress, additional algorithms must be designed and integrated into the identification procedure. Therefore, the traditional method is ineffective in dealing with large quantities of inspected images with diverse distresses, and is incapable of accurately classifying pavement distresses.

Recent advances in machine learning methods have facilitated the investigation of image recognition. Various machine learning methods have been proposed to effectively detect, segment, and classify specific targets in heterogeneous images [4]. Among the machine learning methods, the convolutional neural network (CNN), which is a typical deep learning approach, has proven to be an effective tool for dealing with target identification issues because of its unique local connection and weight sharing features [5]. A CNN can efficiently extract features from an input image through basic procedures, including convolution, pooling, and activation, which significantly improves the accuracy and efficiency of target detection and classification [6]. Following the basic framework of CNN, a growing number of improved CNN-based networks, for example, AlexNet [7], VGG [8], GoogLeNet [9], ResNet [10], and DenseNet [11], have been established to continuously expand the types of identification targets and promote identification accuracy. Improved CNN-based networks have been widely used in engineering practice in many fields because of their distinguished performance in rapid estimation [12] and real-time monitoring [13].

These improved CNN-based networks have been introduced by scholars in the field of pavement distress identification. Kim et al. improved the AlexNet network using transfer learning to make it suitable for five types of distresses detection [14]. Chen et al. proposed a location-aware CNN, consisting of a localization network and a partial cause classification network for detecting potholes, which achieved impressive performance [15]. Li et al. proposed a deep CNN-based method that could automatically classify patches cropped from 3D pavement images with satisfactory performance [16]. NAM et al. proposed a deep CNN-based asphalt pavement crack identification system that could robustly detect and classify pavement cracks in complex background images [17]. Du et al. applied a well-known CNN-based identification algorithm, YOLO, to detect and classify pavement distress, and the results confirmed the high accuracy and efficiency of the method [18]. Zhong et al. proposed a new deep neural network structure, W-SegNet, which is based on multiscale feature fusion and can classify cracks, potholes, and patches with impressive accuracy [19]. Guan et al. developed an automatic pixel-level pavement distress detection framework by integrating stereo vision and deep learning, which showed advantages in terms of accuracy and inference speed over similar methods that segment cracks and potholes from the environment [20]. Liu et al. investigated the influence of image type on the accuracy of different deep learning models, and they found that CNN-based models produced the highest accuracy on fusion images, whereas transfer learning generated the highest accuracy on visible images [21]. Shim et al. proposed a novel neural network structure for detecting pavement distress, and their experimental results showed that this structure could achieve high accuracy with few parameters [22]. Similarly, Mandal et al. proposed an automated pavement distress analysis system based on YOLO v2 [23], and they deployed advanced deep learning algorithms based on different network backbones to detect and characterize pavement distresses [24].

These studies clearly indicate that improved CNN-based methods have very broad prospects for the automatic detection and classification of pavement distress. However, a common limitation of the improved CNN-based methods is that the accuracy relies heavily on the quality of the dataset, which is difficult to ensure in engineering practice [25]. Therefore, generative adversarial networks (GAN) have gained increasing attention from scholars because of their reliability and validity in data augmentation. The GAN can transform random noise and cunningly integrate it into the images to generate realistic-looking images, thereby expanding the sample size and solving the sample imbalance for the dataset [26]. Since its emergence, the original structure of GAN has continued to evolve with the incessant appearance of improved GANs for specific tasks, such as deep convolutional generative adversarial networks (DCGAN) [27], CycleGAN [28], StackGAN [29], and StyleGAN [30]. Improved GANs exhibit satisfactory reliability [31] and intelligence [32] in defect detection tasks [33]. Therefore, recent studies have demonstrated the feasibility and effectiveness of using improved GANs to improve the classification accuracy of pavement distress. Mazzini et al. utilized a GAN to generate new images using a CNN-based texture synthesizer, which was applied to asphalt pavement distress classification model training [34]. Chen et al. compared a dataset enhanced by GAN with an enhanced dataset using traditional methods, and proved that GAN could generate road texture images with better quality, based on which the classification accuracy using DenseNet could be improved significantly [35]. Zhang et al. proposed a crack-patch-only supervised GAN for end-to-end training that was able to avoid the “all-black” phenomenon during the image generation process, and their model achieved exceptional performance for crack datasets [36]. Behzadian et al. established a GAN-based model for pavement distress classification, and their results revealed that the utilization of a GAN increased the F1-score from 0.581 to 0.633 [37]. The utilization of GAN increased the accuracy of pavement distress classification to a higher level. However, at the same time, integration with GAN inevitably posed additional training time and extra computational cost to the classification models, which caused them to drift away from the constraints of practical work. In this context, lightweight GAN has become a critical issue in narrowing the gap between theoretical models and practical requirements.

The basic structure of a GAN consists of a generator and a discriminator, which are essentially composed of several CNNs; hence, the lightweight GAN is regarded as the lightweight issue of the CNNs composing GAN at the primary stage. The representative lightweight methods established in previous studies include the multiscale convolution method used in Inception V1 [9], squeeze and expand method used in SqueezeNet [38], depthwise separable convolution method used in MobileNet [39], Xception [40], and group convolution and channel shuffle operation used in ShuffleNet [41]. Collectively, these studies provided ample alternative lightweight approaches for different procedures comprising the general structure of the GAN. In addition, the studies presented thus far have also provided evidence that different combinations of these lightweight approaches may lead to significant fluctuations in the classification accuracy in different tasks. The major reason is that there is an existing a game process between generator and discriminator, and the lightweight methods implemented on the CNNs could affect the performances of generator and discriminator independently, which may disrupt the balance of the game and ultimately decrease the accuracy of classification models. Therefore, the main challenge faced by researchers is to select the proper lightweight methods for the specific procedures in a GAN model to promote its computational efficiency while maintaining acceptable accuracy when dealing with different classification tasks. However, to the best of our knowledge, very few studies have been found that established lightweight GAN-based models for the classification of pavement distress, which is essential for intelligent pavement monitoring.

To address this research gap, the main aim of this study was to establish a lightweight GAN-based pavement distress classification model that considers both accuracy and efficiency. To recognize multiple pavement distresses in one image, the detection of distresses is a prerequisite. However, considering that this study concentrated on the classification procedure, the situation in which every single image contained only one

pavement distress was focused on. This study began by analyzing the general structure of a GAN composed of various layers, which was designed to enhance the pavement distress image datasets. Therefore, the layers with relatively large parameter quantities were locked as lightweight targets. After examining the structure of the target layers, several potential lightweight methods were proposed and listed as alternative inventories. To explore the most suitable combination of alternative lightweight methods for the GAN-based pavement distress classification model, two groups of comparative experiments named Test-I and Test-II series were conducted, which examined the lightweight degree and classification accuracy, respectively, for the lightweight models. Finally, a lightweight GAN-based model with an optimized structure is proposed based on the experimental results. Compared with previous studies, the present research verified the feasibility of making a lightweight GAN-based model in the field of pavement distress classification. Moreover, optimized lightweight GAN structures considering both computational cost and final classification accuracy were established for the enhancement of pavement distress datasets, which could be recognized as another contribution to the field of intelligent pavement distress classification.

2 Lightweight Process

2.1 Network Structure

Referencing DCGAN [27], a basic GAN structure named Original GAN was designed to generate images with four categories of classification objects, including crack, pothole, patch and background. Original GAN is composed of a generator named Original-G and discriminator named Original-D, as shown in Fig. 1. Convolution kernels with a size of 6 × 6 are applied to the convolution layers and transpose convolution layers. Moreover, batch normalization layers were used to stabilize the training process, and the LeakyReLU(0.02) activation function and sigmoid activation function were assigned to different layers. During the training process, the batch size was set to 32, and the BCE loss function and Adam optimizer were selected to train the GAN at a learning rate of 10^{-5}.

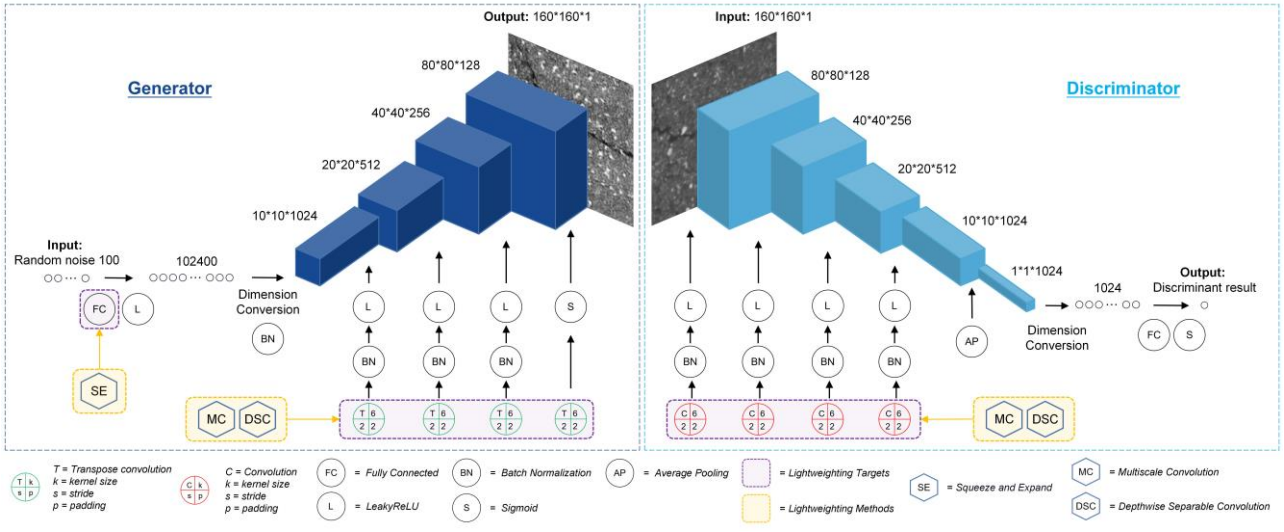

Fig.1 Schematic diagram of Original GAN

To make a GAN lightweight, the most direct approach is to reduce the parameters of the different layers. Therefore, the parameter quantity of the layers in Original-G and Original-D was listed, and then the layers with relatively large parameter quantities was designated as the main targets to be lightweight. The parameter quantities of the layers for Original-G are listed in Table.1. The fully connected layer has a dominant number of parameters

compared to the other layers, which pushes it to the position of the main lightweight target. Although the parameter quantities of the transpose convolution layers were not as large as those of the fully connected layer, the quantities were significantly larger than those of the other layers, and there were four transpose convolution layers in Original-G. Therefore, transpose convolution layers are also recognized as lightweight targets. Taken together, the design of a lightweight structure for the fully connected and transpose convolution layers in Original-G was considered.

No.	Layer	Parameters	No.	Layer	Parameters
1	Fully connected	330,956,800	8	Batch normalization	512
2	LeakyReLU	0	9	LeakyReLU	0
3	Batch normalization	2,048	10	Transpose convolution	1,179,776
4	Transpose convolution	18,874,880	11	Batch normalization	256
5	Batch normalization	1,024	12	LeakyReLU	0
6	LeakyReLU	0	13	Transpose convolution	4609
7	Transpose convolution	4,718,848	14	Sigmoid	0
Total parameter quantity：355,738,753					

Table.1 Parameter quantity of the layers in Original-G

The parameter quantities of the layers in Original-D are listed in Table.2. In contrast to Original-G, only the convolution layers were required to achieve a lightweight design. The other layers contained a very limited number of parameters and thus showed scarce potential to achieve lightweight. Based on this observation, the convolution layers were recognized as lightweight targets, and alternative lightweight methods were selected according to their network structure.

No.	Layer	Parameters	No.	Layer	Parameters
1	Convolution	4,736	9	LeakyReLU	0
2	Batch normalization	256	10	Convolution	18,875,392
3	LeakyReLU	0	11	Batch normalization	2,048
4	Convolution	1,179,904	12	LeakyReLU	0
5	Batch normalization	512	13	Average pooling	0
6	LeakyReLU	0	14	Fully connected	1,025

7	Convolution	4,719,104	15	Sigmoid	0
8	Batch normalization	1024			
Total parameter quantity：24,784,001					

Table.2 Parameter quantities of layers in Original-D

In summary, the fully connected and transpose convolution layers in Original-G and the convolution layers in Original-D were confirmed as lightweight targets. Appropriate lightweight methods were selected as alternatives after analyzing the structural features of the target layers. Considering the structural similarity between transpose convolution layers and convolution layers, their lightweight issues were essentially the same, which means that the alternative lightweight methods for these layers should be identical. Therefore, a general lightweight process can be divided into two steps. First, the lightweight design of the fully connected layer in the Original-G was considered. Squeeze and expand method seemed to be the only reasonable potential method to achieve a light weight for this layer. In the second step, the lightweight design of the transpose convolution layers in Original-G and the convolution layers in Original-D was concentrated on, which followed the same idea. Multiscale convolution, depthwise separable convolution, and the integration of multiscale convolution and depthwise separable convolution constitute an inventory of alternative lightweight methods. To identify the best combination of lightweight methods for Original GAN, comparative experiments were designed and conducted, as described in the following section.

2.2 Lightweight method based on Squeeze and Expand

The squeeze and expand (SE) method, proposed by Iandola et al. [38], was selected as the lightweight method for the fully connected layer in Original-G. By implementing the SE method on the fully connected layer, the number of output nodes was controlled to a small value, which could further reduce the dimensions of the feature maps while retaining their size. During the expansion process, 1 × 1 convolution kernels are designed to restore the dimensions of the feature maps. Specifically, in Original-G, the input nodes of the fully connected layer were reduced from 100 to 1 to compress the random noise input. Moreover, the number of output nodes on the fully connected layer was squeezed from 102,400 to 12,800, and the dimensions of the corresponding feature maps reduced from 1,024 to 128. Subsequently, the dimensions of the squeezed feature maps were expanded to 1,024 by 1 × 1 convolution. A schematic diagram of the lightweight method based on SE used in this study is shown in Fig 2.

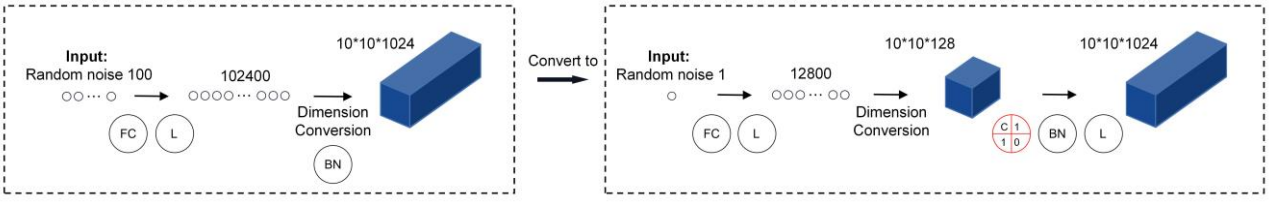

Fig.2 Lightweight process based on SE method

2.3 Lightweight method based on Multiscale Convolution

As for the alternative lightweight methods for the transpose convolution layers in Original-G and the convolution layers in Original-D, the multiscale convolution (MC) method was first considered, which has been proven to be an effective tool to reduce the number of network parameters and improve the network learning

performance [9]. The basic principle is to simultaneously learn the features in feature maps using different convolution kernels with the most appropriate size and reduce the output dimensions of each convolution kernel during convolution and transpose convolution. Subsequently, the tensor concatenation tool can concatenate the output feature maps at the dimension level. In this study, the original 6 × 6 convolution kernels were replaced by 6 × 6 and 4 × 4 convolution kernels for all procedures requiring convolution kernels, and the output dimensions of the convolution kernels after replacement were half of those in the original convolution kernels. Subsequently, the output feature maps extracted by the replaced convolution kernels were concatenated to restore the original dimensions. A schematic of the lightweight method based on the MC used in this research is shown in Fig 3.

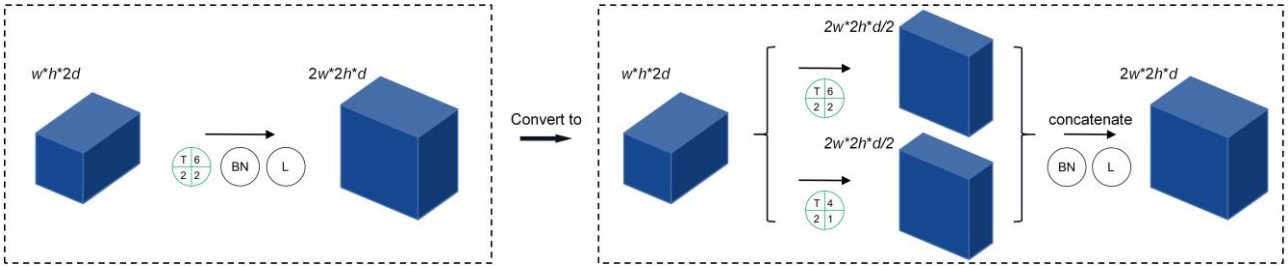

(a) Lightweight of the transpose convolution layers in Original-G

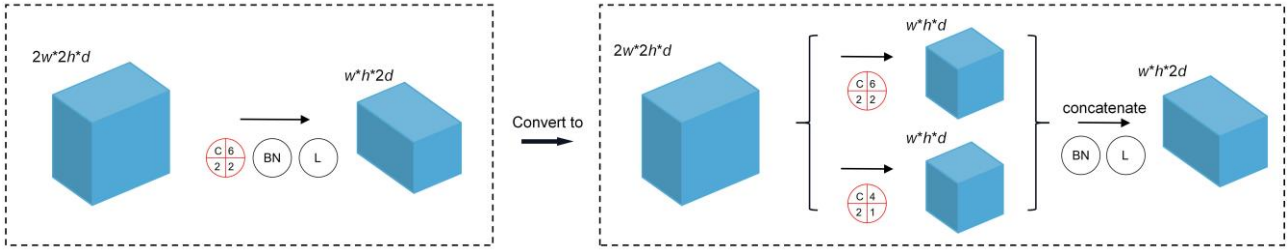

(b) Lightweight of the convolution layers in Original-D

Fig.3 Lightweight process based on MC method

2.4 Lightweight method based on Depthwise Separable Convolution

Depthwise separable convolution (DSC), which has been proven to be an effective approach to reduce model parameters [39], is also an alternative lightweight method for the transpose convolution layers in Original-G and the convolution layers in Original-D. In the convolution and transpose convolution processes, conventional convolution convolved the dimensions and size of feature maps at the same time, which resulted in a large number of parameters. The DSC can separate the convolution process into a channel-by-channel convolution with priority for every feature map and a point-by-point convolution for the entire feature map set, thereby significantly reducing the number of parameters. In this study, the DSC method was implemented on all the transpose convolution and convolution layers. In addition, a batch normalization layer was added before the activation function of the generator output layer to enhance expressiveness. A schematic diagram of the lightweight method based on the DSC used in this study is shown in Fig 4.

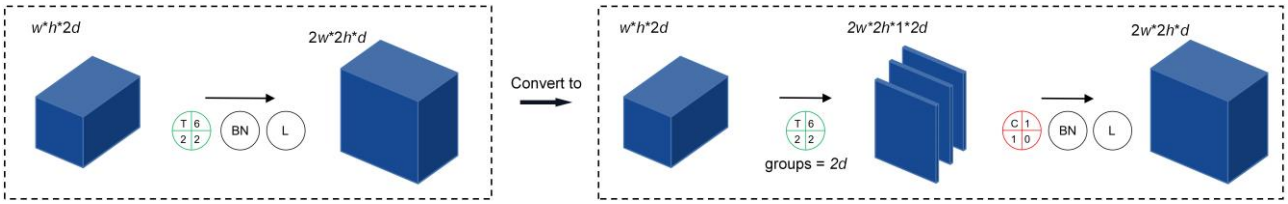

(a) Lightweight of the transpose convolution layers in Original-G

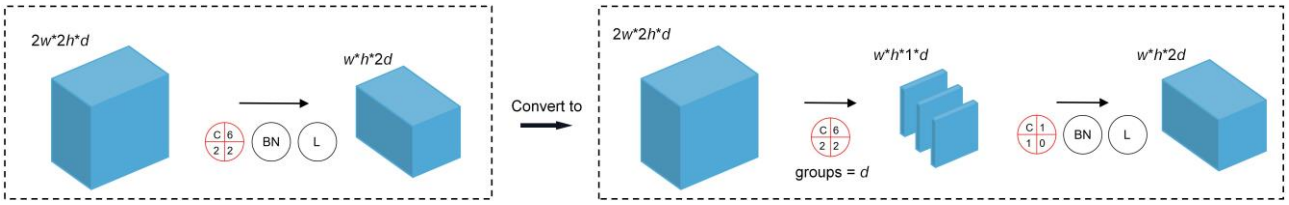

(b) Lightweight of the convolution layers in Original-D

Fig.4 Lightweight process based on DSC method

2.5 Integration of Multiscale Convolution and Depthwise Separable Convolution

In addition to being applied separately, the MC and DSC can be integrated and applied to lightweight targets simultaneously, as represented by the MC&DSC method in this study. In this case, two sets of depthwise separable convolutions for the feature maps were first made, and the convolution kernels of 6 × 6 and 4 × 4 were then used for channel-by-channel convolution. Subsequently, the output dimensions of the subsequent point-by-point convolutions were set to half of the final output dimensions, which were finally concatenated to restore the original dimensions. The MC&DSC process is illustrated in Fig 5.

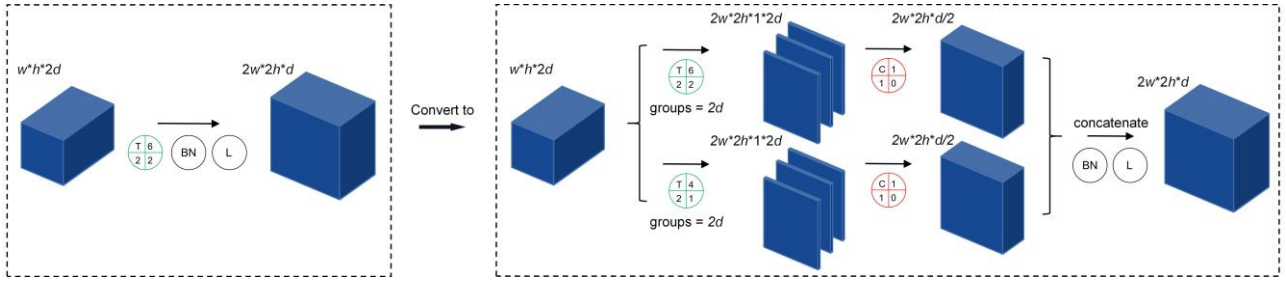

(a) Lightweight of the transpose convolution layers in Original-G

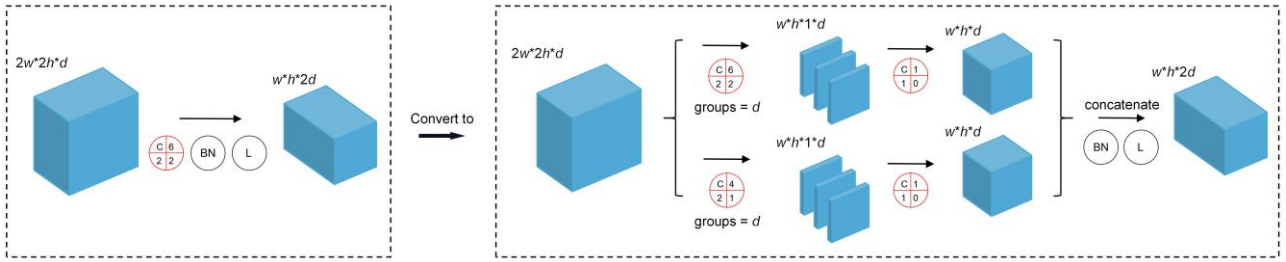

(b) Lightweight of the convolution layers in Original-D

Fig.5 Lightweight process based on MC&DSC

3 Experiment Design

3.1 Dataset

The pavement images used in this study were extracted from the German asphalt pavement distress (GAPs) dataset [42] provided by the Laboratory of Neuroinformatics and Cognitive Robotics at the Technical University of Irmenau in Germany. The images were captured by road inspection vehicles on asphalt pavement, which had a single channel of 160 × 160 pixels. Typical extracted images are shown in Fig.6.

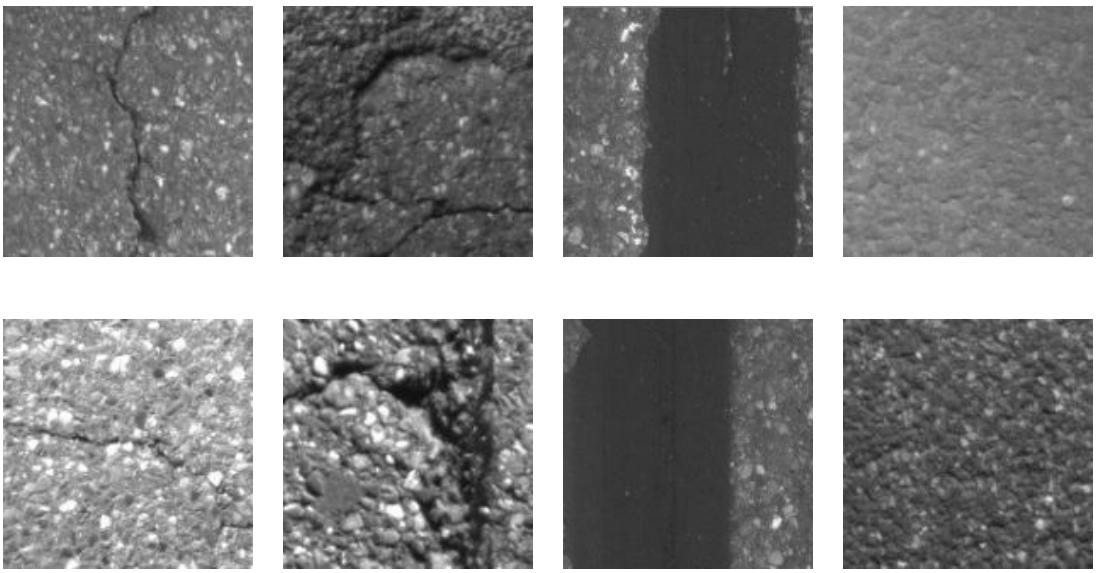

(a) Crack (b) Pothole (c) Patch (d) Background

Fig.6 Typical samples extracted from GAPs

A total of 1,600 images were extracted from GAPs, consisting of four categories: crack, pothole, patch, and pavement background. Each category contained 400 images, of which 60% (240 images) were used as the training set, while the remaining 40% (160 images) were used as the test set. The sample composition of the dataset used in this study is presented in Table.3.

Dataset	Sample size			
	Crack	Pothole	Patch	Background
Original training set for classification model	240	240	240	240
Test set	160	160	160	160
Expanded training set for GANs	1920	1920	1920	1920

Table.3 Sample composition of the datasets consisting of four types of images

It is noteworthy that background noise commonly exists in the images. In addition, the image exposure degrees and distress forms showed significant distinctions even between images of the same category. It could be inferred that the quality of the training set might not qualify to train the GANs to generate satisfactory images. Therefore, the sample size of the training set was expanded eight times using rotation transformation and mirror transformation on the images to construct an expanded training set for GANs. The sample composition of the expanded training set for the GANs is presented in Table.3.

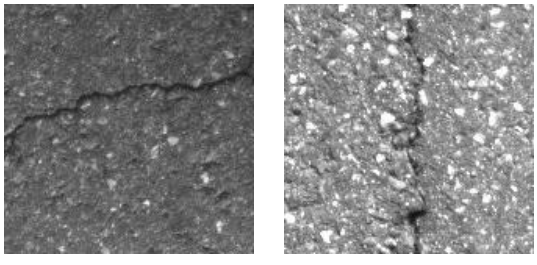

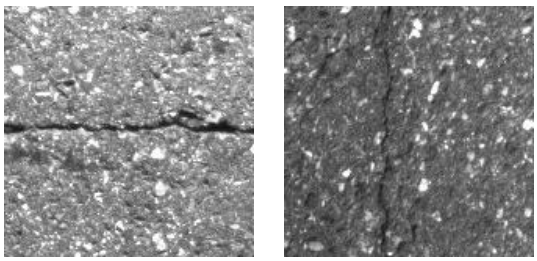

(a) Transverse (b) Longitudinal

Fig.7 Typical samples extracted from GAPs

Considering the actual demand in planning rehabilitations and evaluating the condition of the pavement, the categories of pothole, patch, and background were retained and the crack category was further divided into transverse and longitudinal. Four hundred transverse and longitudinal images each were extracted from the GAPs dataset, and typical samples are shown in Fig.7. Sixty percent (240 images) of the images for each category were used as the training set, whereas the remaining 40% (160 images) were used as the test set. To test the model performance on the reclassification dataset, the sample size of the training set was expanded eight times using noise transformation and mirror transformation on the images. The sample composition of the expanded dataset used in the experiments after the reclassification is presented in Table.4.

Dataset	Sample size				
	Transverse	Longitudinal	Pothole	Patch	Background
Original training set for classification model	240	240	240	240	240
Test set	160	160	160	160	160
Expanded training set for GANs	1920	1920	1920	1920	1920

Table.4 Sample composition of the datasets consisting of five types of images

3.2 Comparative Experiments

Two groups of comparative experiments, namely, Test-I and Test-II series, were designed, as shown in Fig.8, to identify the model with the most suitable lightweight structure for pavement distress classification. Test-I contained 11 experiments that were conducted to examine the data enhancement results of lightweight GANs implementing different methods. The training times and parameter quantities of the lightweight GANs were compared to explore the lightweight effect. In Test-II, after the lightweight GANs with acceptable data enhancement results were selected from Test-I, the dataset enhanced by the lightweight GANs was input to a residual neural network (ResNet) for distress classification. The classification accuracies were compared with the results generated by the model without GAN and Original GAN-based model. Finally, the best model that comprehensively considers the degree of weight and classification accuracy was identified.

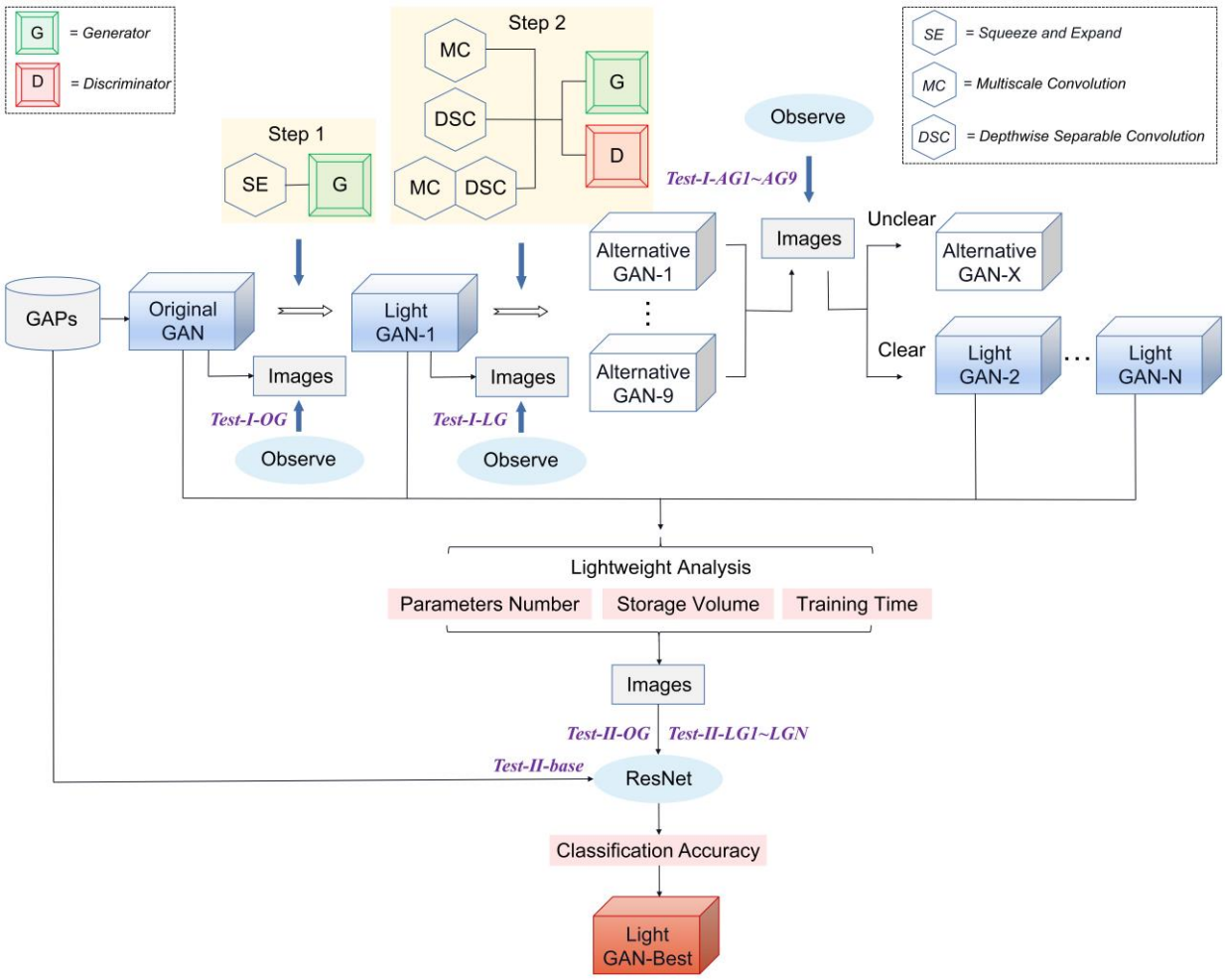

Fig.8 The flow chart of comparative experiments

Specifically, in Test-I, the lightweight version of Original GAN followed two steps. In the first step, the lightweight fully connected layer in Original-G was achieved using the SE method, which constructed the model Light GAN-1. In the second step, a further lightweight was considered based on Light GAN-1. The remaining lightweight targets in Light GAN-1 were the transpose convolution layers of the generator and convolution layers of the discriminator. The alternative methods to achieve lightweight design for the convolution layers and transpose convolution layers were the same, including MC, DSC, and MC&DSC. In summary, three alternative methods for two lightweight targets were developed, which could generate nine different permutations. Therefore, nine corresponding experiments, named Test-I-AG1 to Test-I-AG9, as shown in Table.5, were designed to explore the effectiveness of alternative lightweight GANs with different combinations of lightweight methods. By observing the images generated by the alternative lightweight GANs after training for 1,000 epochs, feasible GANs that could generate relatively high-quality images were sifted for further examination of classification accuracy using ResNet in Test-II. Based on the different classifications of pavement diseases, the experiments were divided into Test-I-a, which was conducted based on four categories of images, including crack, pothole, patch, and background, and Test-I-b, which reclassified the crack images into transverse and longitudinal images. The parameter quantity, storage volume, and training time, which could jointly represent the lightweight degree of the selected feasible GANs, were preliminarily compared with each other and with those of Original GAN as a major result of Test-I.

Experiment	GAN structure	Generator input layer lightweight method	Generator transpose convolution layer lightweight method	Discriminator convolution layer lightweight method
Test-I-OG	Original GAN	/	/	/
Test-I-LG	Light GAN-1	SE	/	/
Test-I-AG1	Alternative GAN-1	SE	MC	MC
Test-I-AG2	Alternative GAN-2	SE	MC	DSC
Test-I-AG3	Alternative GAN-3	SE	MC	MC&DSC
Test-I-AG4	Alternative GAN-4	SE	DSC	MC
Test-I-AG5	Alternative GAN-5	SE	DSC	DSC
Test-I-AG6	Alternative GAN-6	SE	DSC	MC&DSC
Test-I-AG7	Alternative GAN-7	SE	MC&DSC	MC
Test-I-AG8	Alternative GAN-8	SE	MC&DSC	DSC
Test-I-AG9	Alternative GAN-9	SE	MC&DSC	MC&DSC

Table.5 Experiments using different permutations of lightweight methods in Test-I

The main objective of Test-II was to examine the classification accuracy using ResNet trained with the datasets enhanced by lightweight GANs. Test-II-a examined the classification accuracy for four categories of pavement distress, and Test-II-b validated the model performance for classifying five categories of pavement distress, which divided cracks into transverse and longitudinal. In Test-II-a, an experiment named Test-II-a-base was first conducted, which used ResNet trained with the original training set to classify the distress images in the test set. The results of Test-II-a-base were used as a benchmark for classification accuracy in Test-II-a. Then, the alternative lightweight GANs that could generate clear distress images were renamed from Light GAN-1 to Light GAN-n, where the value of n depends on the number of feasible lightweight GANs selected from Test-I-a. The training set for ResNet was successively enhanced by Light GANs from a sample size of 240 to 960, as shown in Table.6, and the classification accuracies with ResNet were obtained from the corresponding experiments of Test-II-a-LG1 to Test-II-a-LGn. Considering that the lightweight process may negatively affect the performance of Original-GAN, an experiment named Test-II-a-OG was also conducted to check the classification accuracy of the ResNet trained with the dataset enhanced by Original-GAN. Finally, by comparing the results generated from the experiments in Test-II-a, the feasibility of using a lightweight GAN-based model for pavement distress classification was validated.

Experiment	Data enhancement method	Sample size of training set				Sample size of test set			
		Crack	Pothole	Patch	Background	Crack	Pothole	Patch	Background

Test-II-a-base	Without GAN	240	240	240	240	160	160	160	160
Test-II-a-OG	Original GAN	960	960	960	960	160	160	160	160
Test-II-a-LG1~ Test-II-a-LGn	Light GAN-1 ~ Light GAN-n	960	960	960	960	160	160	160	160

Table.6 Sample size of the training set and test set for ResNet in Test-II-a

The process of Test-II-b was similar to that of Test-II-a, including experiments without data enhancement and experiments with data enhancement using a lightweight GAN. The components of the training and test sets are presented in Table.7. Based on the results of Test-II-a and Test-II-b, the optimal pavement distress classification model with the most appropriate lightweight structure could be identified comprehensively by considering the lightweight degree and classification accuracy.

Experiment	Data enhancement method	Sample size of training set / test set				
		Transverse	Longitudinal	Pothole	Patch	Background
Test-II-b-base	Without GAN	240/160	240/160	240/160	240/160	240/160
Test-II-b-LG1~ Test-II-b-LGn	Light GAN-1 ~ Light GAN-n	960/160	960/160	960/160	960/160	960/160

Table.7 Sample size of the training set and test set for ResNet in Test-II-b

3.3 Experimental Environment

The experiments were performed on an NVIDIA GeForce RTX 3080 laptop GPU workstation with 16GB RAM. All models were implemented using the deep learning Pytorch library in Python.

4 Result and Discussion

4.1 Data Enhancement with Lightweight GANs

In Test-I-a, the 11 different GANs listed in Table.5 were trained by the expanded training set shown in Table.3 and used to enhance the training set for ResNet, that is, generating the distress images, which means that 11 individual experiments based on different GANs were conducted. In the individual experiments, represented by Test-I-OG to Test-I-AG9 as listed in Table.5, the GANs were trained for 1,000 epochs to generate 720 images for each of these categories, including crack, pothole, patch, and background, followed by a manual visual inspection of the generated images. Table.8 shows the typical generated images used to compare the performance of the GANs, and the models with satisfactory results are highlighted in green. Through careful observation, it was found that the qualities of the images generated by the same GAN for the same category were similar, which means that if the typical image shown in Table.8 is realistic-looking, the other images of this category generated by the same GAN are also clear. In contrast, the unclear images indicated that the images of the same category in that experiment did not reach the standard for data enhancement. Only the GANs that could quickly generate high-quality images for all categories were recognized as capable of data augmentation for the training set of the pavement distress classification model in this study.

Model	Crack	Pothole	Patch	Background
Original GAN	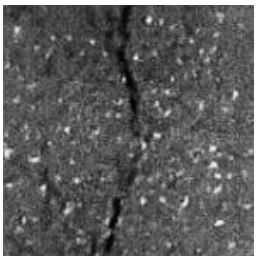	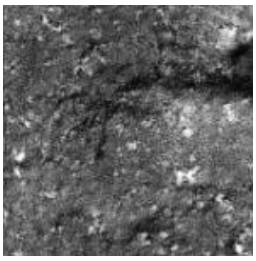	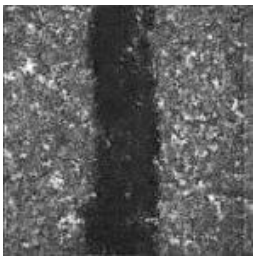	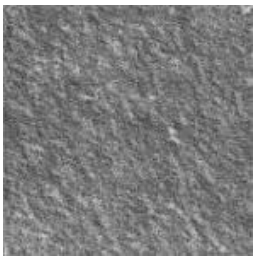
Light GAN-1	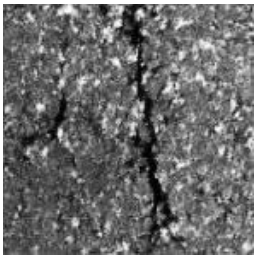	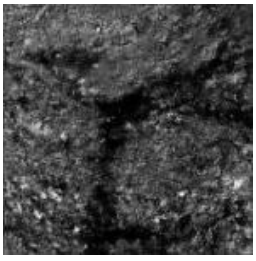	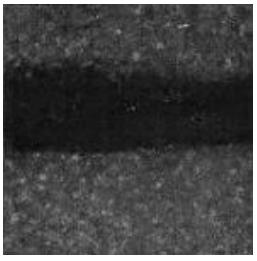	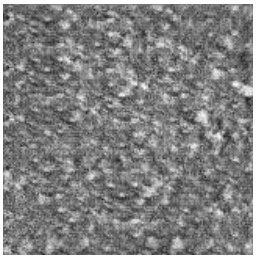
Alternative GAN-1	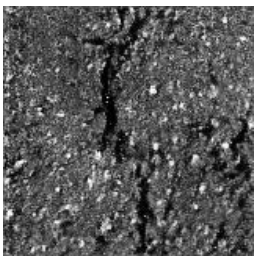	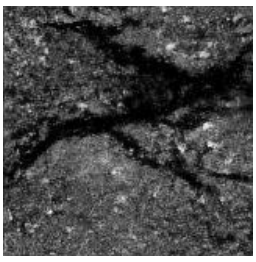	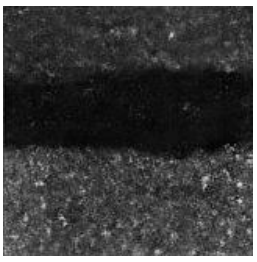	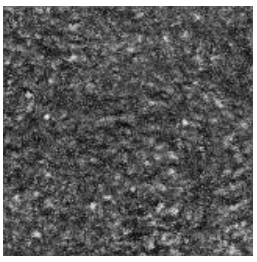
Alternative GAN-2	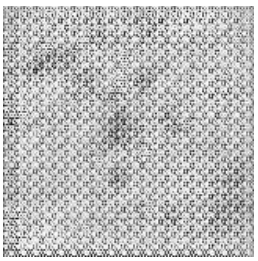	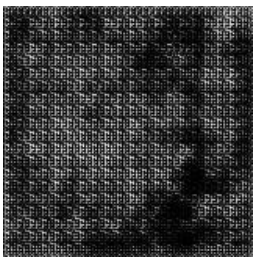	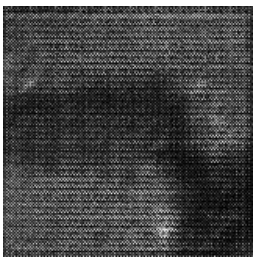	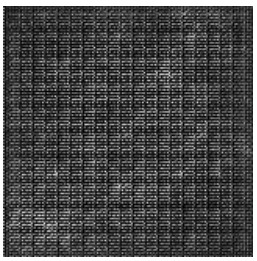
Alternative GAN-3	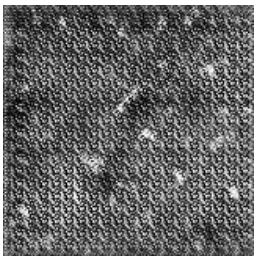	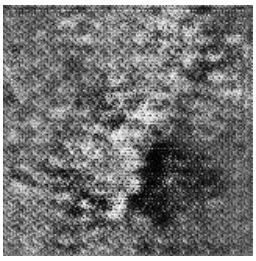	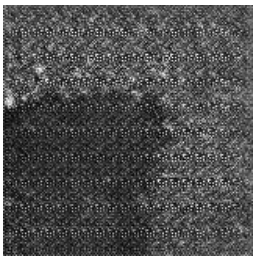	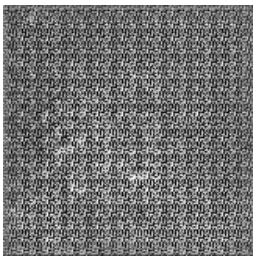
Alternative GAN-4	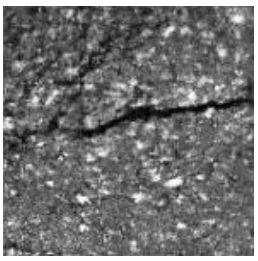	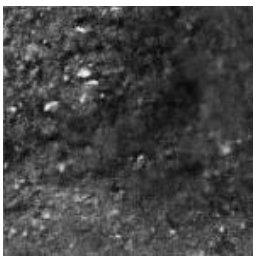	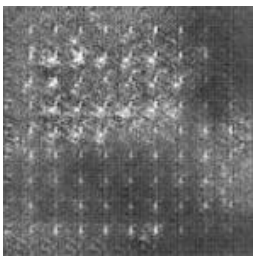	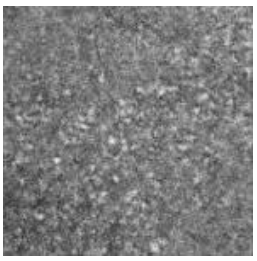

Alternative GAN-5	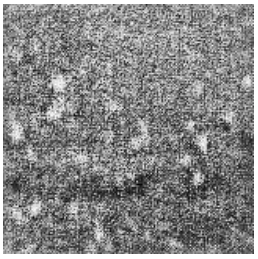	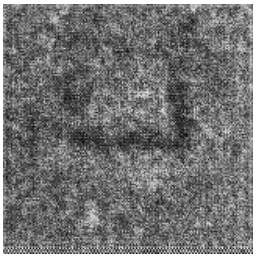	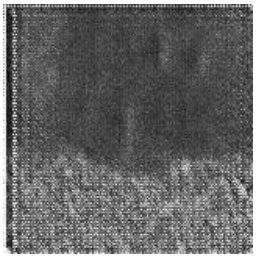	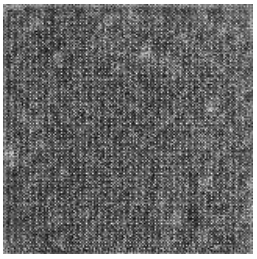
Alternative GAN-6	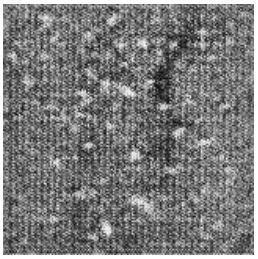	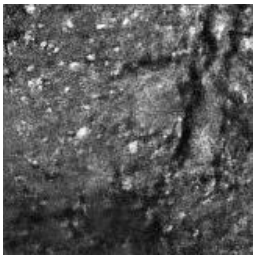	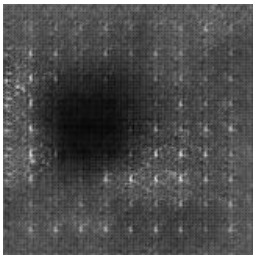	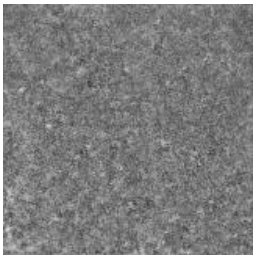
Alternative GAN-7	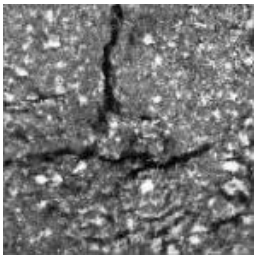	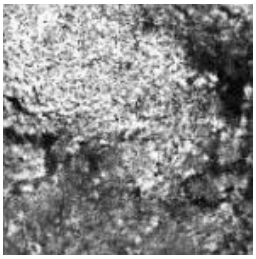	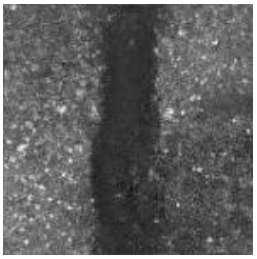	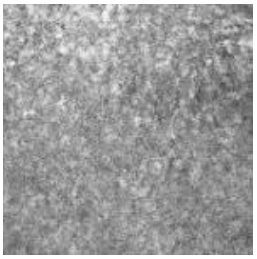
Alternative GAN-8	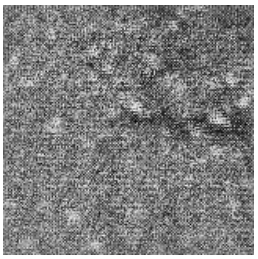	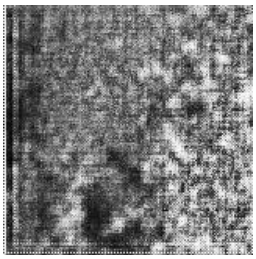	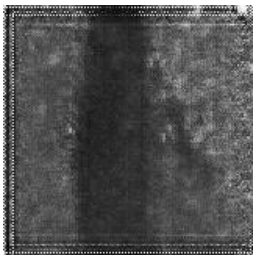	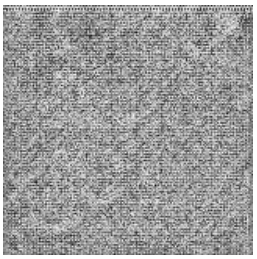
Alternative GAN-9	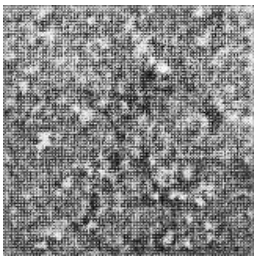	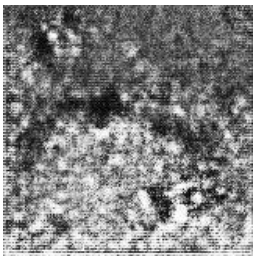	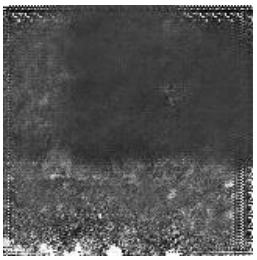	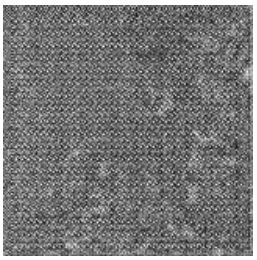

Table.8 Typical images generated by the GANs in Test-I-a

After closer inspection of the experimental results, it can be confirmed that Original GAN can generate satisfactory images for all categories, which proves the effectiveness of Original GAN in enhancing the training set for the classification model. For the lightweight GANs, it is apparent from Table.8 that only a few lightweight GANs could generate realistic-looking images. The positive results generated by Light GAN-1 indicated that the SE of the fully connected layer in Original-G did not exacerbate its performance. Thus, it was reasonable to implement the SE method on all alternative lightweight GANs in Test-I, just as designed in this research. Turning now to the experimental results from Test-I-AG1 to Test-I-AG9, which considered all the permutations of MC, DSC, and MC&DSC, only Alternative GAN-1 (the lightweight GAN implementing MC on both the convolution layers and the transpose convolution layers) and Alternative GAN-7 (the lightweight GAN implementing

MC&DSC on the transpose convolution layers in Original-G and implementing MC on the convolution layers in Original-D) could generate high-quality distress images for all categories. The results of the experiments using other lightweight GANs were unclear for at least one category and thus unacceptable for data enhancement. Alternative GAN-1 and Alternative GAN-7 were successively renamed Light GAN-2 and Light GAN-3, and then their lightweight degree was compared with Original GAN, as shown in Table.9.

Model name		Parameter quantity（$\times 10^6$）			Storage volume（MB）			Training time（h）
Name in Test-I	Renamed after Test-I	Total	Generator	Discriminator	Total	Generator	Discriminator	
Original GAN	Original GAN	380.5	355.7	24.8	4354.8	4071.1	283.7	8.8
Light GAN-1	Light GAN-1	50.5	25.7	24.8	578.2	294.5	283.7	7.1
Alternative GAN-1	Light GAN-2	36.8	18.9	17.9	420.8	215.8	205.0	7.2
Alternative GAN-7	Light GAN-3	19.6	1.7	17.9	225.0	20.0	205.0	7.8

Table.9 Lightweight degree of the GANs sifted by Test-I

Table.9 illustrates that all the lightweight GANs significantly optimized the parameter quantity, storage volume, and training time compared with Original GAN. Among the three sifted lightweight GANs, Light GAN-3 has the lowest value of parameter quantity and storage volume. However, the decrease in parameter quantity and storage volume were not accompanied with a further decrease in training time, which could be found from the comparison between Light GAN-1, Light GAN-2, and Light GAN-3. A possible explanation for the phenomenon is that the DSC increased the network depth, resulting in an increase in the time cost. Therefore, if the lightweight degree is defined based on parameters such as quantity and storage volume, Light GAN-3 has the most effective lightweight structure. According to Test-I, if training time is considered as the main indicator of lightweight degree, the Light GAN-1 seems to be more efficient in terms of computation.

Based on Test-I-a, Test-I-b was designed to examine the generation effect of the transverse and longitudinal directions for Original GAN, Light GAN-1, Light GAN-2, and Light GAN-3. The generation results are presented in Table.10. It was found that Original GAN could not effectively generate realistic transverse and longitudinal directions. One possible reason for this is that the structure of Original GAN used in this study was adjusted according to the four-category scenario. After the reclassification of the crack category into transverse and longitudinal, the extremely obvious characteristics of transverse and longitudinal cause the game between the generator and discriminator to be unbalanced. In contrast, after conducting lightweight methods, the structure of Original GAN changed and could better adapt the transverse and longitudinal characteristics. Consequently, Light GAN-1, Light GAN-2, and Light GAN-3 can generate realistic transverse and longitudinal images, which also

indirectly indicates that these lightweight GANs may be more flexible and applicable to more situations than Original GAN.

Model	Transverse	Longitudinal
Original GAN	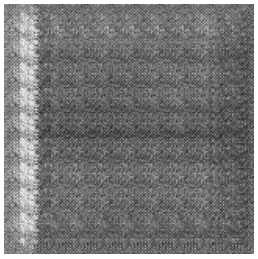	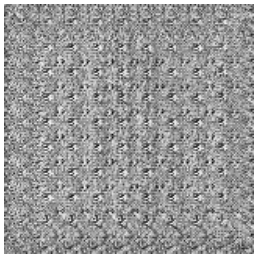
Light GAN-1	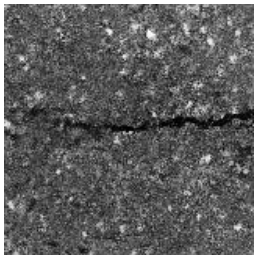	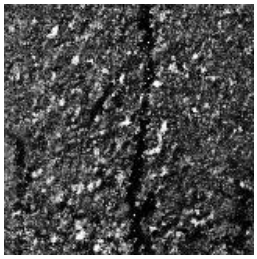
Light GAN-2	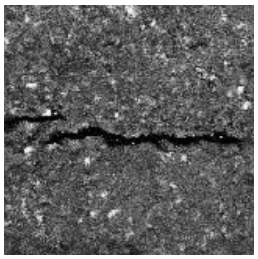	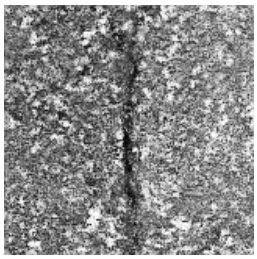
Light GAN-3	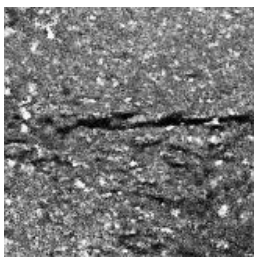	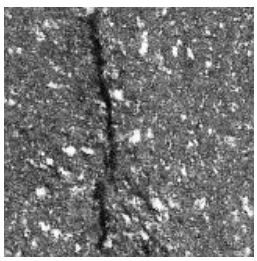

Table.10 Typical images generated by the GANs in Test-I-b

As the performance of a GAN in data enhancement does not necessarily correlate with the performance of the corresponding GAN-based classification model in distress classification, the dataset enhanced by Original GAN, Light GAN-1, Light GAN-2, and Light GAN-3 in Test-II was used as the training set to compare the accuracy of the classification model. Each enhanced training set contained 240 images extracted from the GAPs and 720 images generated by the GAN without manual selection for every category.

4.2 Classification accuracies using ResNet

Test-II was concerned with the accuracy of lightweight GAN-based classification models. Supervised learning for the classification task of four categories of pavement distress, including crack, pothole, patch, and background was first conducted in Test-II-a. ResNet101, a representative ResNet, was successively trained using the original training set, which was enhanced by Original GAN, and the training sets were enhanced by lightweight GANs to conduct the experiments Test-II-a-base, Test-II-a-OG, Test-II-a-LG1, Test-II-a-LG2, and

Test-II-a-LG3. The number of training epochs was set to 200, with a batch size of 1. Adam was used as the optimization algorithm for gradient descent in back propagation, with a learning rate of 10^{-5} and default values of other parameters. The loss function of supervised learning is the BCE function. Accuracy, that is, the proportion of correctly classified samples to the total number of samples in the test set, was adopted as the evaluation index for the performance of the supervised classification models. The accuracy curve, confusion matrix, and loss function curve of the experiments in Test-II are shown in Fig 8.

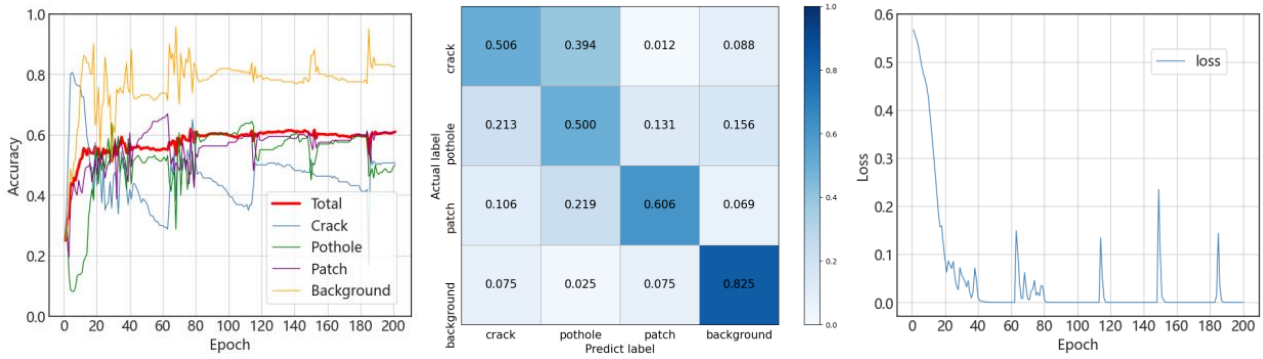

(a) Classification accuracy in Test-II-a-base

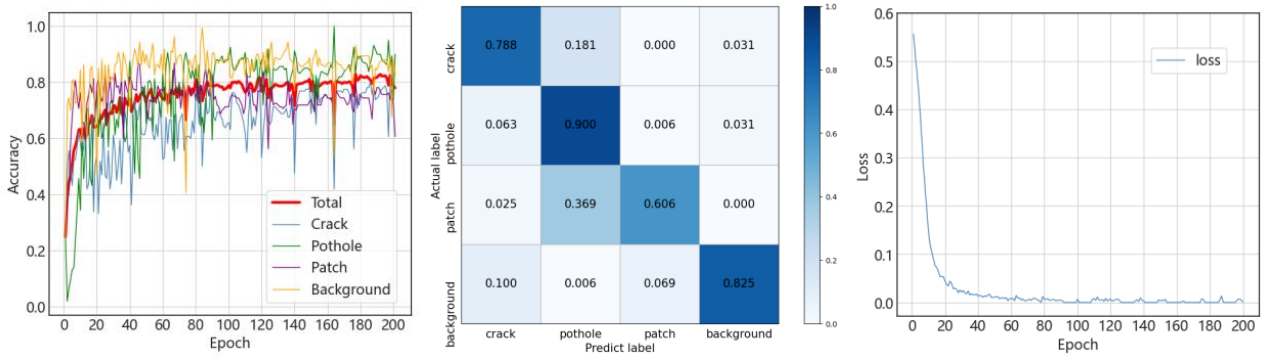

(b) Classification accuracy in Test-II-a-OG

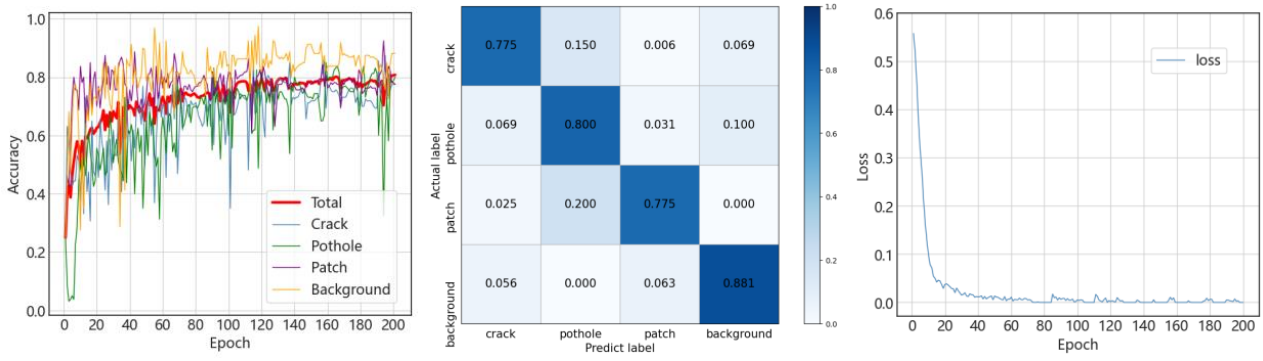

(c) Classification accuracy in Test-II-a-LG1

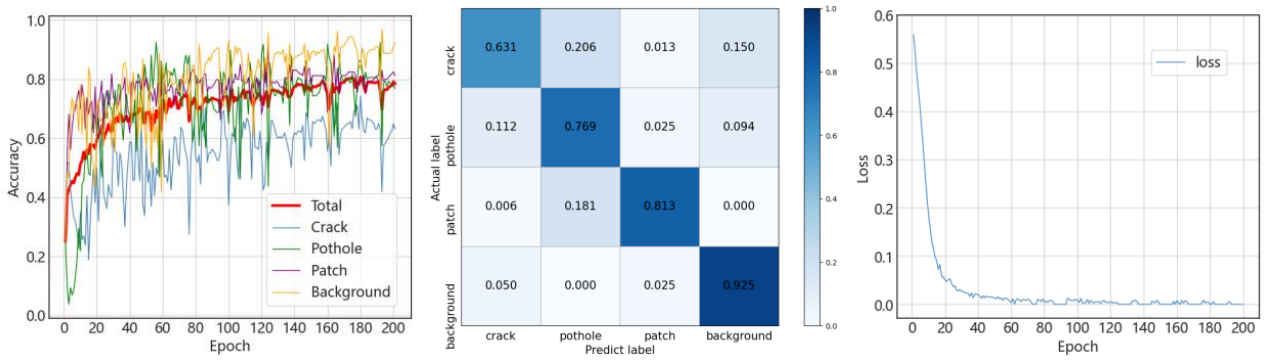

(d) Classification accuracy in Test-II-a-LG2

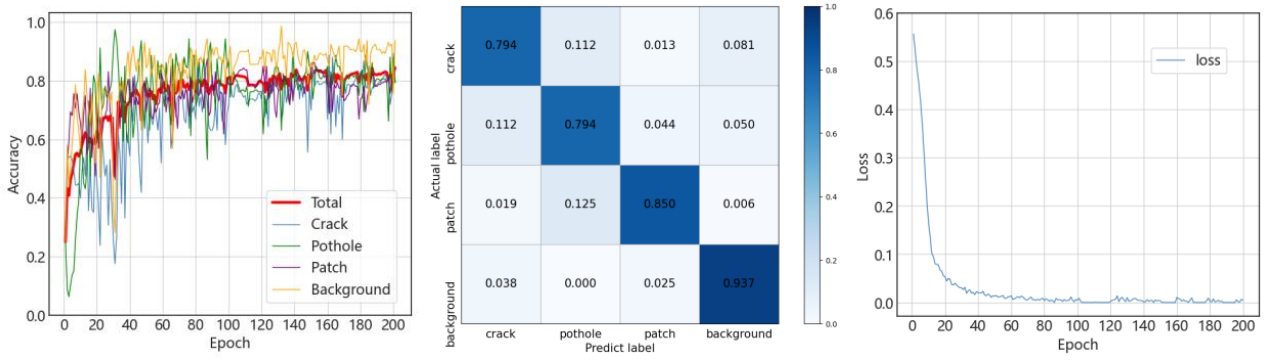

(e) Classification accuracy in Test-II-a-LG3

Fig.9 Pavement distress classification accuracies of the experiments in Test-II-a

As shown in Fig.9(a), the accuracy curves and the loss curve kept spiking during the 200 epochs in Test-II-a-base using the classification model without GAN. Comparatively, Fig.9(b) to Fig.9(e) shows that classification accuracy and loss curves of GAN-based models tended to stabilize within 200 epochs, and the loss curves converged rapidly. To quantitatively analyze the performance of the models in Test-II-a, the classification accuracies for the distress images in the test set after 200 epochs are listed in Table.11.

Classification Model	Classification accuracy on test set（%）				
	Crack	Pothole	Patch	Background	Average
Original ResNet without GAN	50.6	50.0	60.6	82.5	60.9
Original GAN based	78.8	90.0	60.6	82.5	78.0
Light GAN-1 based	77.5	80.0	77.5	88.1	80.8
Light GAN-2 based	63.1	76.9	81.3	92.5	78.4
Light GAN-3 based	79.4	79.4	80.5	93.7	84.4

Table.11 Classification accuracies of the four categories of distress

The results, as shown in Table.11, revealed that training with the datasets enhanced by GANs significantly improved the classification accuracies of the pavement distress images for the ResNet models. A remarkable result was that the lightweight structures improved the classification accuracies of the GAN-based models instead of negatively affecting their performance, which could be found by comparing the classification accuracy of Original

GAN-based model with those of the lightweight GAN-based models. Specifically, Light GAN-1 and Light GAN-2 slightly increased the accuracy of Original GAN-based model by less than 3%, whereas the Light GAN-3 based classification model achieved the most distinguished average accuracy, which was 84.4%.

In Test-II-b, it was further examined that the classification accuracies of the lightweight GAN-based models after the pavement distresses were reclassified into five categories, that is, the crack was divided into transverse and longitudinal. The process of conducting Test-II-b was the same as that of Test-II-a. As shown in Table.12, in the case of the five categories of pavement distress, the lightweight GAN-based models also achieved higher accuracy than the original ResNet model without GAN, similar to the case of the four categories. Among the classification models, the Light GAN-2 based model showed the best performance, improving the average classification accuracy to 87.0%.

Classification Model	Classification accuracy on test set（%）					
	Transverse	Longitudinal	Pothole	Patch	Background	Average
Original ResNet without GAN	75.6	78.1	66.9	61.9	80.6	72.6
Light GAN-1 based	95.6	85.0	72.5	71.9	86.9	82.4
Light GAN-2 based	89.4	93.1	78.7	78.7	95.0	87.0
Light GAN-3 based	89.4	88.7	77.5	77.5	93.8	85.4

Table.12 Classification accuracies of the five categories of distress

Comparing the results of Test-II-a and Test-II-b, the classification model without GAN has better performance in Test-II-b than in Test-II-a, however, the improvement of classification accuracy using lightweight GAN-based models is more significant in Test-II-a. A possible reason is that the characteristics of each category become more significant after the crack is divided into transverse and longitudinal, which naturally reduces the difficulty of classification and reduces the potential for using GAN-based models to improve the classification accuracy. Moreover, compared with the state-of-the-art method published recently [42], which achieved an F1 value of approximately 0.6, it can be concluded that the classification accuracies of approximately 0.8 obtained in Test-II-a and Test-II-b using lightweight GAN-based models are satisfactory.

4.3 Comprehensive comparison

A comprehensive comparison of the model performance is shown in Table.13. The result of the classification model without GAN was listed as the benchmark of test accuracy, whereas the result of Original GAN-based model was selected as the benchmark to evaluate the lightweight degree. According to the results in Table.13, the lightweight GAN-based models improved the classification accuracy of pavement distress by at least 17.5% in the case of four categories and 9.8% in the case of five categories compared with Resnet without GAN. Moreover, all the lightweight structures sifted from Test-I could effectively reduce the parameter quantity, storage volume, and training time of Original GAN. In Light GAN-1, the parameter quantity and storage volume were reduced by 86.7%, the training time was reduced by 19.3%, and the final improvement in classification accuracy was increased by 19.9% and 9.8%, respectively, in four-category and five-category classification tasks. In Light GAN-

2, the parameter quantity and storage volume decreased by 90.3%, training time decreased by 18.2%, and classification accuracy increased by 17.5% in the four-category task and 14.4% in the five-category task. Light GAN-3 reduced the parameter quantity and storage volume by 94.8%, reduced the training time by 11.4%, and increased the classification accuracy by 23.5% for the four-category classification and by 12.8% for the five-category classification. These results confirm that lightweight GAN-based models can effectively classify pavement distress with higher efficiency and even better accuracy compared to the model without GAN and Original GAN-based model. If the parameter quantity and storage volume are mainly considered, implementing SE and MC&DSC on the fully connected layer and the transpose convolution layers, respectively, in the generator, while implementing MC on the convolution layers in the discriminator, is the best lightweight structure. In addition, when the training time is the main factor, the lightweight GAN that only implements SE on the fully connected layer in the generator can achieve an acceptable classification accuracy with less training time.

Classification Model	Parameter quantity		Storage volume		Training time		Test accuracy			
							4 categories		5 categories	
	($\times 10^6$)	reduction (%)	(MB)	reduction (%)	(h)	reduction (%)	(%)	increase (%)	(%)	increase (%)
Without GAN	/	/	/	/	/	/	60.9 (base)	0	72.6 (base)	0
Original GAN based	380.5 (base)	0	4354.8 (base)	0	8.8 (base)	0	78.0	17.1	/	/
Light GAN-1 based	50.5	86.7	578.2	86.7	7.1	19.3	80.8	19.9	82.4	9.8
Light GAN-2 based	36.8	90.3	420.8	90.3	7.2	18.2	78.4	17.5	87.0	14.4
Light GAN-3 based	19.6	94.8	225.0	94.8	7.8	11.4	84.4	23.5	85.4	12.8

Table.13 Comprehensive comparison of lightweight GAN-based classification models

5 Conclusions

This paper described a lightweight GAN-based model used to perform an intelligent classification of pavement distresses based on datasets with small sample sizes. The model also helped explore the optimized lightweight structure considering both lightweight degree and classification accuracy. A DCGAN, together with a ResNet, collectively constructed the basic classification model in this study. For the lightweight methods, the SE method was used to lightweight the fully connected layer in the generator, while the MC method, DSC method, and their integration (MC&DSC) were used to lightweight the transpose convolution layers in the generator and convolution layers in the discriminator. Simultaneously, the different permutations of lightweight methods and

lightweight targets were considered to design experiments to compare the performance of the constructed models. Using two series of comparative experiments, feasible lightweight GAN-based models with optimized structures were proposed to achieve a more efficient and accurate classification of pavement distress. The major findings are summarized as follows:

(1) Although only three of the ten lightweight GANs were verified to be capable of effectively enhancing the dataset of pavement distress images, all three sifted lightweight GANs could significantly reduce the computation cost and training time under the prerequisite of maintaining the classification performance.

(2) In the case where the parameter quantity and storage volume were defined as the main indicators of the lightweight degree, the lightweight GAN-based model with the structure of SE implemented on the fully connected layer, MC&DSC implemented on the transpose convolution layers in the generator, and MC implemented on the convolution layers in the discriminator achieved the best performance, decreasing the computation cost by 94.8% and increasing the classification accuracy by 23.5% in four distress category tasks and 12.8% in five distress category tasks.

(3) If the main factor is the training time, the single use of the SE method to the fully connected layer in the generator is the best choice according to the results of this study, which could save 19.3% of the training time for the learning process of GAN and could still achieve satisfactory accuracies of 80.8% for the four-category classification and 82.4% for the five-category classification by integrating the lightweight GAN with the ResNet-based classification model.

In summary, the feasibility and effectiveness of a lightweight GAN-based model for pavement distress classification were verified with sufficient evidence in this research. The insights gained from this study may assist in the development of novel intelligent pavement monitoring tools with better adaptability for engineering practice, and we hope that this research can, to some extent, narrow the gap between theoretical research and practical engineering requirements in the field of intelligent monitoring of pavement distress. As this is the first study of substantial duration that attempts to make the GAN-based pavement distress classification model lightweight, it has also raised a number of questions that require further investigation.

First, only a limited number of pavement distress categories were considered in this study. Although the crack category was divided into transverse and longitudinal to enhance the applicability of the proposed approach, it may still not be capable of directly supporting engineering practice considering the complex condition of the real pavement and the actual requirements of planning rehabilitation. Thus, a natural progression of this work is to expand the classification target for further optimization of GAN-based models. In particular, the classification of the alligator and block will be considered.

Moreover, this study considered only the automatic classification of pavement distress. The proposed lightweight models may not be able to constitute an intelligent pavement distress recognition system independently. This is because in engineering practice, most pavement images contain more than one distress, and the distress needs to be first detected as a prerequisite for automatic classification. Therefore, an advanced lightweight automatic detection algorithm should be developed and integrated with classification models to meet the requirements of practical pavement inspection and maintenance.

In addition, making the layers in the GAN lightweight directly is focused in this study. However, there are other routes for the distress classification model, such as the transfer-learning approach. Several transfer learning-based approaches for pavement distress recognition have been proposed in recent studies, such as the models established by Hou [43], Li [44], and Liu [45], which also achieved impressive performance. Considerably more work will be needed to make comprehensive comparisons among the models following different lightweight routes to discuss their unique advantages as well as the feasibility of integrating these lightweight models.

Finally, it was found that the lightweight model with the lowest computational cost and that with minimum

time cost were not the same. This is a rather interesting phenomenon that might be related to the depth of the network and the internal computational logic of the algorithm. Further research is needed to examine the links between the model structure and computational efficiency, which could provide support for engineers to adjust the algorithm according to the network structure. Thus, a higher classification efficiency can be expected, which is essential for pushing the theoretical models closer to the application in pavement inspection works.

Acknowledgement

This work was supported by the Opening Project Fund of Materials Service Safety Assessment Facilities (MSAF-2021-109), Key Science and Technology Projects in the Transportation Industry in 2021 (2021-ZD2-047), 2021 Science and Technology Innovation Project of Shandong Hi-Speed Group (SDGS-2021-0472-2), and the National Natural Science Foundation of China (Grant no. 51708026).

References

[1] N.T. Sy, M. Avila, S. Begot, J.C. Bardet, IEEE, Detection of Defects in Road Surface by a Vision System, IEEE Mediterranean Electrotechnical Conference, Ajaccio, FRANCE, 2008, pp.847-851. DOI:10.1109/MELCON.2008.4618541

[2] Y.F. Liu, S.J. Cho, B.F. Spencer, J.S. Fan, Automated assessment of cracks on concrete surfaces using adaptive digital image processing, Smart Structures and Systems 14(4) (2014), pp.719-741. DOI:10.12989/sss.2014.14.4.719

[3] Y.C. Huang, Y.C. Tsai, Dynamic Programming and Connected Component Analysis for an Enhanced Pavement Distress Segmentation Algorithm, Transportation Research Record (2225) (2011), pp.89-98. DOI:10.3141/2225-10

[4] A. Aboah, M. Shoman, V. Mandal, S. Davami, Y. Adu-Gyamfi, A. Sharma, I.C. Soc, A Vision-based System for Traffic Anomaly Detection using Deep Learning and Decision Trees, IEEE/CVF Conference on Computer Vision and Pattern Recognition (CVPR), Electr Network, 2021, pp.4202-4207. DOI:10.1109/CVPRW53098.2021.00475

[5] Y. Hou, Q.H. Li, C. Zhang, G.Y. Lu, Z.J. Ye, Y.H. Chen, L.B. Wang, D.D. Cao, The State-of-the-Art Review on Applications of Intrusive Sensing, Image Processing Techniques, and Machine Learning Methods in Pavement Monitoring and Analysis, Engineering 7(6) (2021), pp.845-856. DOI:10.1016/j.eng.2020.07.030

[6] V. Mandal, A.R. Mussah, P. Jin, Y. Adu-Gyamfi, Artificial Intelligence-Enabled Traffic Monitoring System, Sustainability 12(21) (2020), 9177. DOI:10.3390/su12219177

[7] A. Krizhevsky, I. Sutskever, G.E. Hinton, ImageNet Classification with Deep Convolutional Neural Networks, Communications of the ACM 60(6) (2017), pp.84-90. DOI:10.1145/3065386

[8] K. Simonyan, A.J.C.S. Zisserman, Very Deep Convolutional Networks for Large-Scale Image Recognition, arXiv preprint arXiv:1409.1556 (2014). https://doi.org/10.48550/arXiv.1409.1556

[9] C. Szegedy, W. Liu, Y.Q. Jia, P. Sermanet, S. Reed, D. Anguelov, D. Erhan, V. Vanhoucke, A. Rabinovich, IEEE, Going Deeper with Convolutions, IEEE Conference on Computer Vision and Pattern Recognition (CVPR), Boston, MA, 2015, pp.1-9. DOI:10.1109/CVPR.2015.7298594

[10] K.M. He, X.Y. Zhang, S.Q. Ren, J. Sun, IEEE, Deep Residual Learning for Image Recognition, 2016 IEEE Conference on Computer Vision and Pattern Recognition (CVPR), Seattle, WA, 2016, pp.770-778. DOI:10.1109/CVPR.2016.90

[11] G. Huang, Z. Liu, L. van der Maaten, K.Q. Weinberger, IEEE, Densely Connected Convolutional Networks,

30th IEEE/CVF Conference on Computer Vision and Pattern Recognition (CVPR), Honolulu, HI, 2017, pp.2261-2269. DOI:10.1109/CVPR.2017.243
[12] Z.H. Weng, G. Ablat, D.F. Wu, C.L. Liu, F. Li, Y.C. Du, J. Cao, Rapid pavement aggregate gradation estimation based on 3D data using a multi-feature fusion network, Automation in Construction 134 (2022) 104050. DOI:10.1016/j.autcon.2021.104050
[13] D. Wang, B.Y. Ren, B. Cui, J.J. Wang, X.L. Wang, T. Guan, Real-time monitoring for vibration quality of fresh concrete using convolutional neural networks and IoT technology, Automation in Construction 123 (2021) 103510. DOI:10.1016/j.autcon.2020.103510
[14] B. Kim, S. Cho, Automated Vision-Based Detection of Cracks on Concrete Surfaces Using a Deep Learning Technique, Sensors 18(10) (2018) 3452. DOI:10.3390/s18103452
[15] H.S. Chen, M.H. Yao, Q.L. Gu, Pothole detection using location-aware convolutional neural networks, International Journal of Machine Learning and Cybernetics 11(4) (2020) pp.899-911. DOI:10.1007/s13042-020-01078-7
[16] B.X. Li, K.C.P. Wang, A. Zhang, E.H. Yang, G.L. Wang, Automatic classification of pavement crack using deep convolutional neural network, International Journal of Pavement Engineering 21(4) (2020) pp.457-463. DOI:10.1080/10298436.2018.1485917
[17] N.A.M. Yusof, M.K. Osman, M.H.M. Noor, A. Ibrahim, N.M. Tahir, N.M. Yusof, IEEE, Crack Detection and Classification in Asphalt Pavement Images using Deep Convolution Neural Network, 8th IEEE International Conference on Control System, Computing and Engineering (ICCSCE), Batu Ferringhi, MALAYSIA, 2018, pp. 227-232. DOI:10.1109/ICCSCE.2018.8685007
[18] Y.C. Du, N. Pan, Z.H. Xu, F.W. Deng, Y. Shen, H. Kang, Pavement distress detection and classification based on YOLO network, International Journal of Pavement Engineering 22(13) (2021) pp.1659-1672. DOI:10.1080/10298436.2020.1714047
[19] J.T. Zhong, J.Q. Zhu, J. Huyan, T. Ma, W.G. Zhang, Multi-scale feature fusion network for pixel-level pavement distress detection, Automation in Construction 141 (2022) 104436. DOI:10.1016/j.autcon.2022.104436
[20] J.C. Guan, X. Yang, L. Ding, X.Y. Cheng, V.C.S. Lee, C. Jin, Automated pixel-level pavement distress detection based on stereo vision and deep learning, Automation in Construction 129 (2021) 103788. DOI:10.1016/j.autcon.2021.103788
[21] F.Y. Liu, J. Liu, L.B. Wang, Deep learning and infrared thermography for asphalt pavement crack severity classification, Automation in Construction 140 (2022) 104383. DOI:10.1016/j.autcon.2022.104383
[22] S. Shim, J. Kim, S.W. Lee, G.C. Cho, Road surface damage detection based on hierarchical architecture using lightweight auto-encoder network, Automation in Construction 130 (2021) 103833. DOI:10.1016/j.autcon.2021.103833
[23] V. Mandal, L. Uong, Y. Adu-Gyamfi, Automated Road Crack Detection Using Deep Convolutional Neural Networks, IEEE International Conference on Big Data (Big Data), Seattle, WA, 2018, pp. 5212-5215. DOI:10.1109/BigData.2018.8622327
[24] V. Mandal, A.R. Mussah, Y. Adu-Gyamfi, Deep Learning Frameworks for Pavement Distress Classification: A Comparative Analysis, 8th IEEE International Conference on Big Data (Big Data), 2020, pp. 5577-5583. DOI:10.1109/bigdata50022.2020.9378047
[25] D. Hu, J.J. Chen, S. Li, Reconstructing unseen spaces in collapsed structures for search and rescue via deep learning based radargram inversion, Automation in Construction 140 (2022) 104380. DOI:10.1016/j.autcon.2022.104380
[26] I.J. Goodfellow, J. Pouget-Abadie, M. Mirza, B. Xu, D. Warde-Farley, S. Ozair, A. Courville, Y. Bengio,

Generative Adversarial Nets, 28th Conference on Neural Information Processing Systems (NIPS), Montreal, CANADA, 2014, pp. 2672-2680. DOI:10.1145/3422622
[27] A. Radford, L. Metz, S.J.C.e. Chintala, Unsupervised Representation Learning with Deep Convolutional Generative Adversarial Networks, arXiv preprint arXiv:1511.06434, 2015. https://doi.org/10.48550/arXiv.1511.06434
[28] J.Y. Zhu, T. Park, P. Isola, A.A. Efros, IEEE, Unpaired Image-to-Image Translation using Cycle-Consistent Adversarial Networks, 16th IEEE International Conference on Computer Vision (ICCV), Venice, ITALY, 2017, pp.2242-2251. DOI:10.1109/ICCV.2017.244
[29] H. Zhang, T. Xu, H.S. Li, S.T. Zhang, X.G. Wang, X.L. Huang, D. Metaxas, IEEE, StackGAN: Text to Photo-realistic Image Synthesis with Stacked Generative Adversarial Networks, 16th IEEE International Conference on Computer Vision (ICCV), Venice, ITALY, 2017, pp.5908-5916. DOI:10.1109/ICCV.2017.629
[30] T. Karras, S. Laine, T. Aila, I.C. Soc, A Style-Based Generator Architecture for Generative Adversarial Networks, IEEE/CVF Conference on Computer Vision and Pattern Recognition (CVPR), Long Beach, CA, 2019, pp.4396-4405. DOI:10.1109/CVPR.2019.00453
[31] S. Bang, F. Baek, S. Park, W. Kim, H. Kim, Image augmentation to improve construction resource detection using generative adversarial networks, cut-and-paste, and image transformation techniques, Automation in Construction 115 (2020) 103198. DOI:10.1016/j.autcon.2020.103198
[32] W.J. Liao, X.Z. Lu, Y.L. Huang, Z. Zheng, Y.Q. Lin, Automated structural design of shear wall residential buildings using generative adversarial networks, Automation in Construction 132 (2021) 103931. DOI:10.1016/j.autcon.2021.103931
[33] G.W. Zhang, Y. Pan, L.M. Zhang, Semi-supervised learning with GAN for automatic defect detection from images, Automation in Construction 128 (2021) 103764. DOI:10.1016/j.autcon.2021.103764
[34] D. Mazzini, P. Napoletano, F. Piccoli, R. Schettini, A Novel Approach to Data Augmentation for Pavement Distress Segmentation, Computers in Industry 121 (2020) 103225. DOI:10.1016/j.compind.2020.103225
[35] N. Chen, Z.J. Xu, Z. Liu, Y.H. Chen, Y.H. Miao, Q.H. Li, Y. Hou, L.B. Wang, Data Augmentation and Intelligent Recognition in Pavement Texture Using a Deep Learning, IEEE Transactions on Intelligent Transportation Systems (2022). DOI:10.1109/TITS.2022.3140586
[36] K.G. Zhang, Y.T. Zhang, H.D. Cheng, CrackGAN: Pavement Crack Detection Using Partially Accurate Ground Truths Based on Generative Adversarial Learning, IEEE Transactions on Intelligent Transportation Systems 22(2) (2021) pp.1306-1319. DOI:10.1109/TITS.2020.2990703
[37] Ashkan Behzadian, Tanner Wambui Muturi, Tianjie Zhang, Hongmin Kim, Amanda Mullins, Yang Lu, Neema Jasika Owor, Yaw Adu-Gyamfi, William Buttlar, Majidifard Hamed, Armstrong Aboah, David Mensching, Spragg Robert, Matthew Corrigan, Jack Youtchef, Dave Eshan, The 1st Data Science for Pavements Challenge, https://arxiv.org/pdf/2206.04874.pdf
[38] F.N. Iandola, S. Han, M.W. Moskewicz, K. Ashraf, W.J. Dally, K. Keutzer, SqueezeNet: AlexNet-level accuracy with 50x fewer parameters and <0.5MB model size, arXiv preprint arXiv:1602.07360 (2016). https://doi.org/10.48550/arXiv.1602.07360
[39] A.G. Howard, M. Zhu, B. Chen, D. Kalenichenko, W. Wang, T. Weyand, M. Andreetto, H. Adam, MobileNets: Efficient Convolutional Neural Networks for Mobile Vision Applications, arXiv preprint arXiv:1704.04861 (2017). https://doi.org/10.48550/arXiv.1704.04861
[40] F. Chollet, IEEE, Xception: Deep Learning with Depthwise Separable Convolutions, 30th IEEE/CVF Conference on Computer Vision and Pattern Recognition (CVPR), Honolulu, HI, 2017, pp.1800-1807. DOI:10.1109/CVPR.2017.195
[41] X. Zhang, X.Y. Zhou, M.X. Lin, R. Sun, IEEE, ShuffleNet: An Extremely Efficient Convolutional Neural

Network for Mobile Devices, 31st IEEE/CVF Conference on Computer Vision and Pattern Recognition (CVPR), Salt Lake City, UT, 2018, pp.6848-6856. DOI:10.1109/CVPR.2018.00716

[42] R. Snicker, M. Eisenbach, M. Sesselmann, K. Debes, H.M. Gross, IEEE, Improving Visual Road Condition Assessment by Extensive Experiments on the Extended GAPs Dataset, International Joint Conference on Neural Networks (IJCNN), Budapest, HUNGARY, 2019. pp.1-8. DOI:10.1109/IJCNN.2019.8852257

[43] Y. Hou, H.Y. Shi, N. Chen, Z. Liu, H. Wei, Q. Han, Vision Image Monitoring on Transportation Infrastructures: A Lightweight Transfer Learning Approach, IEEE Transactions on Intelligent Transportation Systems (2022). DOI:10.1109/TITS.2022.3150536

[44] Y.S. Li, P.Y. Che, C.L. Liu, D.F. Wu, Y.C. Du, Cross-scene pavement distress detection by a novel transfer learning framework, Computer-Aided Civil and Infrastructure Engineering 36(11) (2021) pp.1398-1415. DOI:10.1111/mice.12674

[45] F.Y. Liu, Z.J. Ye, L.B. Wang, Deep transfer learning-based vehicle classification by asphalt pavement vibration, Construction and Building Materials 342 (2022). DOI:10.1016/j.conbuildmat.2022.127997